

Density matrix reconstruction using non-negative matrix product states

Donghong Han,¹ Chu Guo,^{2,*} and Xiaoting Wang^{1,†}

¹*Institute of Fundamental and Frontier Sciences,*

University of Electronic Science and Technology of China, Chengdu, 610051, China

²*Key Laboratory of Low-Dimensional Quantum Structures and Quantum Control of Ministry of Education,*

Department of Physics and Synergetic Innovation Center for Quantum Effects and Applications,

Hunan Normal University, Changsha 410081, China

(Dated: April 27, 2022)

Quantum state tomography is a central technique for quantum information processing, but is challenging due to the exponential growth of its complexity with the system size. In this work, we propose an algorithm which iteratively finds the best non-negative matrix product state approximation based on a set of measurement outcomes whose size does not necessarily grow exponentially. Compared to the tomography approach based on neural network states, our scheme utilizes a so-called tensor train representation that allows straightforward recovery of the unknown density matrix in matrix product state form. As applications, our algorithm is numerically demonstrated for the ground state of the XXZ spin chain under depolarization noise.

Introduction – Characterizing an unknown quantum state is of central importance in developing quantum technologies. Standard quantum state tomography (QST) reconstructs a generic quantum state by performing projective measurements on an informationally complete basis [1, 2]. The number of projective measurements required grows exponentially with the system size. In the meantime, current quantum technologies have pushed the number of qubits to close to one hundred [3–5], and scalable quantum state tomography schemes are greatly in need. With additional assumptions on the underlying quantum state, more efficient schemes than the standard QST have been proposed. For example, QST for a sparse quantum state by compressive sensing [6–9], QST for quantum states which are permutationally invariant [10, 11], and QST for quantum states which can be efficiently represented with a low-depth parametric quantum circuit [12]. In particular, QST based on tensor network representation [13, 14] as well as neural network ansatz [15–19] is a promising approach to extend QST to a much larger scale, which has both been demonstrated on several tens of qubits based on synthetic data.

For pure quantum states of size L which can be well approximated by matrix product states (MPS), it has been proven that a set of $O(L)$ local n -body reduced density matrices suffices to exactly reconstruct the global quantum state, where n is a constant if the target state has a bounded entanglement. Thus only a polynomial number of quantum measurements are required [13, 14]. It has also been shown later that a similar approach could also be applied to reconstructing density matrices, with an additional assumption of the *invertibility* of the underlying mixed quantum state [20]. However, such methods based on local density matrices are not easy to implement in practice since 1) exact tomography of a series of local density matrices may be already hard, and 2) we can only reconstruct an approximation of each local density matrix from tomography using a finite number of mea-

surements, and the approximation errors could accumulate and affect the overall tomography performance of the entire state. Another method based on an MPS ansatz is proposed using an unsupervised machine learning algorithm in [21], where only global measurement data on a randomly prepared basis are required. Such method however only considers the reconstruction of pure states.

In contrast to the tensor network based approach where the unknown quantum states are directly parameterized using tensor networks whose parameters are then updated based on measurement data, QST based on neural network states models the distribution of the quantum measurement outcomes as classical neural network works, which has been applied for both pure states as vectors [15, 22] and for mixed states as density matrices [16, 17]. One important difference is that the latter approach directly deals with probability distributions that are real and non-negative. A possible drawback of the neural network states based methods is that it is not clear which neural network representation is suitable for a given unknown quantum state. Moreover, the outcome of the latter approach is a neural network representing the probability distribution of the measurement outcomes under the given state, instead of the state itself. It would generally be exponentially hard to further reconstruct the state as a vector or a density matrix from the probability distribution.

We note that the concept of MPS has also been adapted to represent the multi-variant probability distribution function, in which context it is referred to as tensor train representation [23]. Motivated by this, we propose a QST scheme that combines the advantages of both the tensor network approach and the neural network approach. Specifically, in the first stage, a tensor train representation of the multi-variant distribution function is constructed based on the quantum measurement data, instead of a neural network representation, and a density matrix renormalization group (DMRG)-

like algorithm is used to find the optimal tensor train representation. After that, the tensor train is transformed back into a matrix product operator (MPO) representation of the unknown density matrix. Compared to QST based on tensor network states, our scheme directly uses a tensor train representation for the multi-variate probability distribution function, instead of the unknown density matrix; compared to QST based on neural network states, our scheme constructs the unknown density matrix as an MPO, which allows efficient evaluation of its entries.

Method – In this work, we consider quantum measurements given by informationally complete positive-operator valued measures (POVMs) [24–26], which describes the most general quantum measurements allowed by quantum theory [27]. We denote the single qubit POVM as $\{M^a\}$, where M^a is positive semi-definite satisfying $\sum_a M^a = I$ (I denotes the identity matrix). For a single qubit, a minimal informationally complete POVM can be chosen as $M^a = \frac{1}{2} |\psi^a\rangle\langle\psi^a|$ with

$$\begin{aligned} |\psi^0\rangle &= |0\rangle \\ |\psi^1\rangle &= \sqrt{\frac{1}{3}} |0\rangle + \sqrt{\frac{2}{3}} |1\rangle \\ |\psi^2\rangle &= \sqrt{\frac{1}{3}} |0\rangle + \sqrt{\frac{2}{3}} e^{i\frac{2\pi}{3}} |1\rangle \\ |\psi^3\rangle &= \sqrt{\frac{1}{3}} |0\rangle + \sqrt{\frac{2}{3}} e^{i\frac{4\pi}{3}} |1\rangle, \end{aligned} \quad (1)$$

which form the vertices of a regular tetrahedron in the Bloch sphere [28]. Such a single-qubit POVM, $\mathbf{M} = \{M^a\}_{a=0,1,2,3}$ can be viewed as a 3-dimensional tensor written as $M_{\sigma,\sigma'}^a$ with two physical indices σ, σ' of dimension 2 and another index a of dimension 4 corresponding to different measurement outcomes. If we reshape the single-qubit density matrix into a vector of size 4, then \mathbf{M} becomes a 4×4 invertible matrix, representing a one-to-one mapping between the density matrix and the single-qubit probability distribution.

As in [17], for an L -qubit quantum system, we consider the quantum measurement defined by

$$M^{\otimes \mathbf{a}} \equiv M^{a_1} \otimes M^{a_2} \otimes \cdots \otimes M^{a_L}, \quad (2)$$

where $\mathbf{a} = (a_1, \dots, a_L)$ represents a string of integers specifying the local projectors, and each integer $a_l \in \{0, 1, 2, 3\}$. The probability distribution $P(\mathbf{a})$ forms an L -variable distribution function in which each local dimension d is equal to 4, satisfying $P(\mathbf{a}) \geq 0$ and $\sum_a P(\mathbf{a}) = 1$. Interestingly, if we assume that the unknown quantum state $\hat{\rho}$ can be efficiently represented as an MPO

$$\hat{\rho} = \sum_{b_1, b_2, \dots, b_{L+1}} W_{b_1, b_2}^{\sigma_1, \sigma'_1} W_{b_2, b_3}^{\sigma_2, \sigma'_2} \cdots W_{b_L, b_{L+1}}^{\sigma_L, \sigma'_L}, \quad (3)$$

where b_l denotes the auxiliary indices, then $P(\mathbf{a})$ can be written as an MPS

$$P(\mathbf{a}) = \sum_{b_1, b_2, \dots, b_{L+1}} X_{b_1, b_2}^{a_1} X_{b_2, b_3}^{a_2} \cdots X_{b_L, b_{L+1}}^{a_L}, \quad (4)$$

with each tensor $X_{b_l, b_{l+1}}^{a_l} = \sum_{\sigma_l, \sigma'_l} W_{b_l, b_{l+1}}^{\sigma_l, \sigma'_l} M_{\sigma_l, \sigma'_l}^{a_l}$. Therefore the bond dimensions of $P(\mathbf{a})$, which are defined as the dimension of the auxiliary indices $D_l = \dim(b_l)$, are exactly the same as the bond dimensions of $\hat{\rho}$. Since \mathbf{M} is invertible, we can efficiently transform back and forth between the density matrix $\hat{\rho}$ and the probability distribution $P(\mathbf{a})$. Here we choose to first construct $P(\mathbf{a})$ as an MPS, and then transform it back into a density matrix. One advantage of this approach is that as long as the constructed $P(\mathbf{a})$ is a proper probability distribution, then the density matrix $\hat{\rho}$ from this approach will automatically be Hermitian (which however may not be positive if there are not enough measurement data).

Thus the problem reduces to reconstructing an approximate probability distribution $P_s(\mathbf{a})$, based on a set of N samples $\mathbf{a}^1, \mathbf{a}^2, \dots, \mathbf{a}^N$ collected from experiment. Assuming among those samples there are only N_s different ones, which are still denoted as $\mathbf{a}^1, \mathbf{a}^2, \dots, \mathbf{a}^{N_s}$, where each distinct sample \mathbf{a}^j has multiplicity n_j , each \mathbf{a}^j appears with a probability $P_s(\mathbf{a}^j) = \frac{n_j}{N}$, $j = 1, \dots, N_s$. $P_s(\mathbf{a}^j)$ will eventually converge to the exact distribution $P(\mathbf{a})$ as N increases. For a limited number of samples, the entries of $P_s(\mathbf{a})$ are approximately equal to the corresponding entries of $P(\mathbf{a})$. Therefore the original QST is reduced to the following mathematical problem: given some approximated values of the nonzero elements of an unknown $P(\mathbf{a})$, can we construct a tensor train approximation of $P(\mathbf{a})$ with a minimum bond dimension D ?

To this end, we note that each sample \mathbf{a}^j can be encoded as a *one hot* MPS as

$$\mathbf{a}^j \mapsto A^j = \sum_{c_a, c_2, \dots, c_{L+1}} A_{j, c_1, c_2}^{a_1} A_{j, c_2, c_3}^{a_2} \cdots A_{j, c_L, c_{L+1}}^{a_L}, \quad (5)$$

such that $\dim(c_l) = 1$ for all $1 \leq l \leq L$, and each tensor $A_{j, c_l, c_{l+1}}^{a_l}$ satisfies $A_{j, 0, 0}^{a_l} = 1$ iff a_l equals to the l -th element of \mathbf{a}^j , and otherwise 0. For example, if the l -th element of \mathbf{a}^j is 3 then the l -th element on the right hand side of Eq. (5), $A_{j, c_l, c_{l+1}}^{a_l}$, satisfies that $A_{j, 0, 0}^0 = 0$, $A_{j, 0, 0}^1 = 0$, $A_{j, 0, 0}^2 = 0$ and $A_{j, 0, 0}^3 = 1$. With Eq. (5) we can rewrite the probability distribution formed by N samples as

$$P_s(\mathbf{a}) = \sum_{j=1}^{N_s} \frac{n_j}{N} A^j. \quad (6)$$

$P_s(\mathbf{a})$ can be viewed as a superposition of the one hot states A^j , weighted by its multiplicity. $P_s(\mathbf{a})$ can be directly taken as the best approximation of $P(\mathbf{a})$, that is, setting $P(\mathbf{a}) = P_s(\mathbf{a})$, $P_s(\mathbf{a})$ can be directly evaluated

from Eq. (6) using simple MPS arithmetics. However, given a limited set of samples, the bond dimension of the resulting MPS could be much larger than that of the target distribution. Moreover, this might result in an over-fitting problem, since $P_s(\mathbf{a})$ will be perfect for known samples but will be 0 for unknown samples. For better efficiency and generalizability, one can search for $P(\mathbf{a})$ which is approximately equal to $P_s(\mathbf{a})$ under the condition that the bond dimension is bounded by a fixed value D . This could be done in two approaches [29]: 1) evaluating Eq. (6) exactly and then compressing the resulting MPS using SVD, and 2) iteratively searching for the solution to the following optimization problem

$$\text{Loss}(P(\mathbf{a})) \equiv \sum_{j=1}^{N_s} \|P(\mathbf{a}) - P_s(\mathbf{a})\|^2, \quad (7)$$

with a maximum bond dimension D , where $\|P\|$ means the Frobenius norm of the tensor P . We will follow the latter approach which is more precise in practice. One complication here is that if one directly uses the approaches in [29], the MPS ansatz will be kept in a canonical form by iteratively using either singular value decomposition (SVD) or QR decomposition, and the solution generally contains negative values, which is undesirable for a probability distribution. To ensure the nonnegativity of $P(\mathbf{a})$, one could represent $P(\mathbf{a})$ as a nonnegative MPS instead, that is, each tensor X in Eq. (4) is nonnegative. Several algorithms have been proposed to approximate a target probability distribution using a nonnegative MPS with a fixed bond dimension [30,31,32]. Here we use a refined approach based on [32], the central idea of which is to use a non-negative matrix decomposition instead of SVD or QR decomposition.

Specifically, we first define the following tensors $X_{b_{k+1};a_{k+1},\dots,a_L}^{>k}$ and $X_{a_1,\dots,a_{k-1};b_k}^{<k}$:

$$X^{>k} = \sum_{b_{k+2},\dots,b_{L+1}} X_{b_{k+1},b_{k+2}}^{a_{k+1}} \dots X_{b_{L+1},b_L}^{a_L}; \quad (8)$$

$$X^{<k} = \sum_{b_1,\dots,b_{k-1}} X_{b_1,b_2}^{a_1} \dots X_{b_{k-1},b_k}^{a_{k-1}}, \quad (9)$$

and $G_{b_{k+1},b'_{k+1}}^{>k}, G_{b_k,b'_k}^{<k}$

$$G^{>k} = \sum_{a_{k+1},\dots,a_L} X_{b_{k+1};a_{k+1},\dots,a_L}^{>k} X_{b'_{k+1};a_{k+1},\dots,a_L}^{>k}; \quad (10)$$

$$G^{<k} = \sum_{a_1,\dots,a_{k-1}} X_{a_1,\dots,a_{k-1};b_k}^{<k} X_{a_1,\dots,a_{k-1};b'_k}^{<k}, \quad (11)$$

With Eqs.(8) and (9) we can rewrite $P(\mathbf{a})$ as

$$P(\mathbf{a}) = \sum_{b_k,b_{k+1}} X_{b_k,b_{k+1}}^{a_k} X_{\dots,a_{k-1};b_k}^{<k} X_{b_{k+1};a_{k+1},\dots}^{>k}, \quad (12)$$

for each $1 \leq k \leq L$. Substituting Eq. (12) into Eq. (7), we can see that the loss function has the form

$\|V - WH\|^2$, with $V \leftarrow P_s(\mathbf{a})$, $W \leftarrow X_{a_k,a_{k+1}}^{a_k}$ and $H \leftarrow X_{\dots,a_{k-1};b_k}^{<k} X_{b_{k+1};a_{k+1},\dots}^{>k}$. Thus the goal becomes to find the best non-negative factorization of V . One of the most well known approaches for solving this problem is the following updating rule

$$W \leftarrow W \circ \frac{[VH^t]}{W H H^t}; \quad (13)$$

$$H \leftarrow H \circ \frac{[W^t V]}{W^T W H}, \quad (14)$$

where \circ means Hadmard (element-wise) product and $\frac{[A]}{[B]}$ denotes the element-wise division of the matrices A and B . With Eqs.(13) and (14) the loss function is guaranteed to decrease monotonically [33]. From Eq. (13), one can update the tensor $X_{b_k,b_{k+1}}^{a_k}$ as

$$X_{b_k,b_{k+1}}^{a_k} \leftarrow X_{b_k,b_{k+1}}^{a_k} \circ \frac{[\sum_{a_l \neq k} P_s(\mathbf{a}) X^{<k} X^{>k}]}{[\sum_{b'_k,b'_{k+1}} X_{b'_k,b'_{k+1}}^{a_k} G_{b_{k+1},b'_{k+1}}^{>k} G_{b_k,b'_k}^{<k}]} \quad (15)$$

The denominator on the right hand side of Eq. (15) can be efficiently evaluated without computing the summation in Eq. (6), for which we define two tensors $\tilde{G}_{j,b_{k+1},c_{k+1}}^{>k}$ and $\tilde{G}_{j,b_k,c_k}^{<k}$:

$$\tilde{G}_j^{>k} = \sum_{a_{k+1},\dots,a_L} X_{b_{k+1};a_{k+1},\dots,a_L}^{>k} A_{j,c_{k+1};a_{k+1},\dots,a_L}^{>k}; \quad (16)$$

$$\tilde{G}_j^{<k} = \sum_{a_1,\dots,a_{k-1}} X_{a_1,\dots,a_{k-1};b_k}^{<k} A_{j,a_1,\dots,a_{k-1};c_k}^{<k}, \quad (17)$$

where $A^{>k}$ and $A^{<k}$ are defined similar to Eq. (8) and (9). Then we have

$$\begin{aligned} & \sum_{a_l \neq k} P_s(\mathbf{a}) X^{<k} X^{>k} \\ &= \sum_j \frac{n_j}{N} \sum_{b'_k,b'_{k+1}} A_{c_k,c_{k+1}}^{a_k} \tilde{G}_{j,b_{k+1},c_{k+1}}^{>k} \tilde{G}_{j,b_k,c_k}^{<k}. \end{aligned} \quad (18)$$

Thus, the complete algorithm to minimize the loss function $\text{Loss}(P(\mathbf{a}))$ in Eq. (7) is shown in Algorithm.1.

Algorithm 1 Nonnegative Tensor Train State Tomography

Input: the set of samples from POVM measurement;
Output: near-optimal non-negative MPS form of $P(\mathbf{a})$;

- 1: Encode each \mathbf{a}^j into A^j according to Eq. (5);
- 2: Randomly initialize $P(\mathbf{a})$ as in [34];
- 3: **for** $k = L, L-1, \dots, 2$ **do**
- 4: $G_{b_{k+1},b'_{k+1}}^{>k} = \sum_{a_{k+1},b_{k+2},b'_{k+2}} G_{b_{k+2},b'_{k+2}}^{>k+1} X_{b_{k+1},b_{k+2}}^{a_{k+1}} X_{b'_{k+1},b'_{k+2}}^{a_{k+1}}$;
- 5: **for** $j = 1, 2, \dots, N_s$ **do**
- 6: $G_{b_{k+1},c_{k+1}}^{>k} = \sum_{a_{k+1},b_{k+2},c_{k+2}} \tilde{G}_{j,b_{k+2},c_{k+2}}^{>k+1} X_{b_{k+1},b_{k+2}}^{a_{k+1}} A_{c_{k+1},c_{k+2}}^{a_{k+1}}$;
- 7: **end for**

```

8: end for
9: while true do
10:   for  $k = 1, 2, \dots, L-1$  do
11:     update  $X_{b_k, b_{k+1}}^{a_k}$  using Eq. (15);
12:      $G_{b_{k+1}, b'_{k+1}}^{<k+1} = \sum_{a_k, b_k, b'_k} G_{b_k, b'_k}^{<k} X_{b_k, b_{k+1}}^{a_k} X_{b'_k, b'_{k+1}}^{a_k};$ 
13:     for  $j = 1, 2, \dots, N_s$  do
14:        $G_{j, b_{k+1}, c_{k+1}}^{<k+1} =$ 
15:          $\sum_{a_k, b_k, c_k} \tilde{G}_{j, b_k, c_k}^{<k} X_{b_k, b_{k+1}}^{a_k} A_{c_k, c_{k+1}}^{a_k};$ 
16:     end for
17:   end for
18:   for  $k = L, L-1, \dots, 2$  do
19:     update  $X_{b_{k+1}, b_{k+2}}^{a_{k+1}}$  using Eq. (15);
20:      $G_{b_{k+1}, b'_{k+1}}^{>k} =$ 
21:        $\sum_{a_{k+1}, b_{k+2}, b'_{k+2}} G_{b_{k+2}, b'_{k+2}}^{>k+1} X_{b_{k+1}, b_{k+2}}^{a_{k+1}} X_{b'_{k+1}, b'_{k+2}}^{a_{k+1}};$ 
22:     for  $j = 1, 2, \dots, N_s$  do
23:        $G_{j, b_{k+1}, c_{k+1}}^{>k} =$ 
24:          $\sum_{a_{k+1}, b_{k+2}, c_{k+2}} \tilde{G}_{j, b_{k+2}, c_{k+2}}^{>k+1} X_{b_{k+1}, b_{k+2}}^{a_{k+1}} A_{c_{k+1}, c_{k+2}}^{a_{k+1}};$ 
25:     end for
26:   end for
27:   if stopping criterion is meet then
28:     break;
29:   end if
30: end while
31: return  $P(\mathbf{a})$ 

```

Results – We demonstrate our algorithm by reconstructing the density matrix corresponding to the ground state of the XXZ chain subjecting to depolarization noise. The Hamiltonian of the XXZ chain can be written as

$$\hat{H} = \sum_{l=1}^{L-1} J(\hat{\sigma}_l^x \hat{\sigma}_{l+1}^x + \hat{\sigma}_l^y \hat{\sigma}_{l+1}^y + \gamma \hat{\sigma}_l^z \hat{\sigma}_{l+1}^z) + h \sum_{l=1}^L \hat{\sigma}_l^z, \quad (19)$$

where L is the number of spins of the system, J is the tunneling strength which we fix to 1, h is the magnetization strength and γ is the interaction strength. We choose $h = 1$ to break the degeneracy of the ground state due to the spin flip symmetry. The depolarization noise is described by the CPTP map:

$$\hat{\rho} \rightarrow \mathcal{E}(\hat{\rho}) = \frac{p\hat{I}}{d} + (1-p)\hat{\rho}, \quad (20)$$

with d as the Hilbert space size ($d = 2^L$ in our case), \hat{I} the identity operator, $\hat{\rho}$ the density matrix corresponding to the exact ground state, and p the strength of the noise. Here we note that for $p = 0$, namely for pure states, there already exists efficient MPS-based tomography algorithm which directly use MPS as the ansatz to represent an unknown pure state [13].

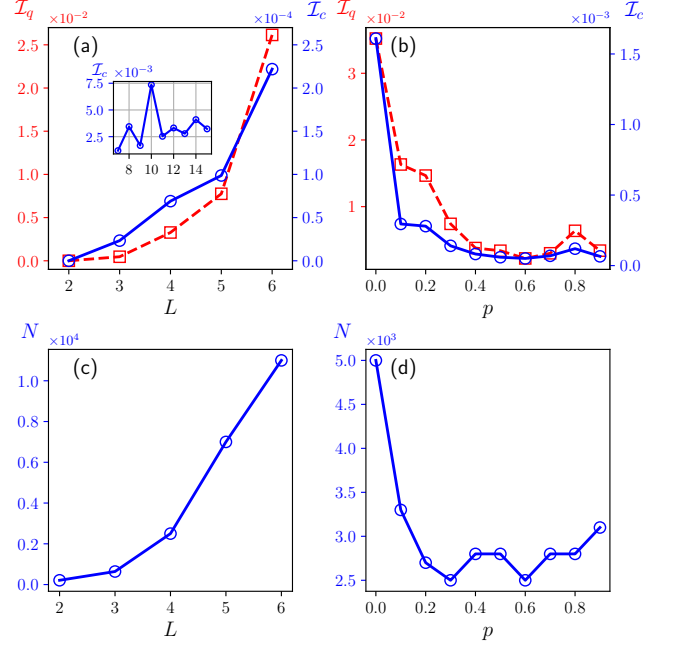


FIG. 1. (a) \mathcal{I}_q (red dashed line with squares) and \mathcal{I}_c (blue solid line with circles) as functions of system size L for fixed $p = 0.6$. The inset shows \mathcal{I}_c as a function of system size for larger system size (\mathcal{I}_c for $L > 6$ is not shown since it is too expensive to compute). (b) \mathcal{I}_q and \mathcal{I}_c as functions of depolarized noise intensity p for fixed $L = 4$. (c) The minimum number of required training data N as a function of L such that $\mathcal{I}_c \leq 1\%$, with $p = 0.6$. (d) The minimum number of required training data N as a function of p such that $\mathcal{I}_c \leq 1\%$, with $L = 4$. All simulations are done with a bond dimension $D = 10$.

Similar to [17], we use both the quantum fidelity and the classical fidelity to measure the learning accuracy. Specifically, the quantum fidelity is defined as

$$\mathcal{F}_q = \text{tr}^2 \left(\sqrt{\sqrt{\hat{\rho}} \hat{\sigma} \sqrt{\hat{\rho}}} \right), \quad (21)$$

for two density matrices $\hat{\rho}$ and $\hat{\sigma}$, and the classical fidelity is defined as

$$\mathcal{F}_c = \mathbb{E}_{a \sim P} [\sqrt{P_m(\mathbf{a})/P_i(\mathbf{a})}], \quad (22)$$

where $P_m(\mathbf{a})$ is the measured probability distribution, and $P_i(\mathbf{a})$ is the ideal probability distribution. We also define the quantum and the classical infidelities as $\mathcal{I}_q = 1 - \mathcal{F}_q$ and $\mathcal{I}_c = 1 - \mathcal{F}_c$ respectively. In our numerical simulations, we have generated two independent synthetic datasets for each parameter setting we have considered, each with 30,000,000 samples. One dataset is used for training and the other is used for testing. For the quantum fidelity, we directly compute \mathcal{F}_q between the reconstructed density matrix and the target density matrix. For the classical fidelity, we use a test dataset to evaluate Eq. (22).

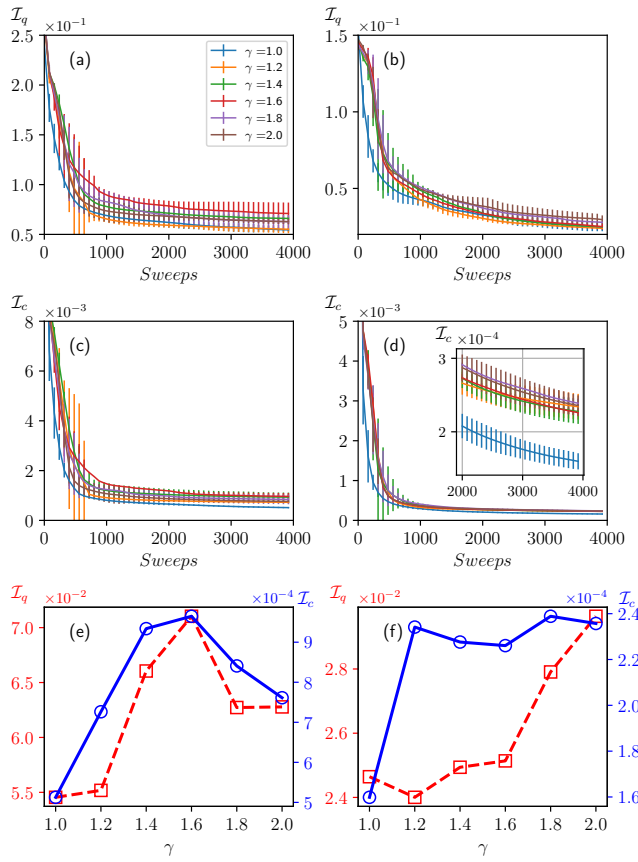


FIG. 2. (a, c) \mathcal{I}_q (a) and \mathcal{I}_c (c) as functions of the number of sweeps for different γ s with $p = 0.4$. (b, d) \mathcal{I}_q (b) and \mathcal{I}_c (d) as functions of the number of sweeps for different γ s with $p = 0.6$. The inset in (d) shows the tail of the convergence of \mathcal{I}_c . In (a, b, c, d) we have chosen 5 best results according to their loss values out of 100 trials and plotted the mean values of them (The standard deviations are shown as error bars). (e) The left and right axis show the final \mathcal{I}_q and \mathcal{I}_c as functions of γ with $p = 0.4$. (f) The left and right axis show the final \mathcal{I}_q and \mathcal{I}_c as functions of γ with $p = 0.6$. Here we have chosen $L = 6$ and used $N_{\text{train}} = 30000000$.

We first study the final reconstruction quality as a function of the system size L and the noise strength p . We show \mathcal{I}_q and \mathcal{I}_c as functions of L in Fig. 1(a) and of p in Fig. 1(b) respectively. We can see that the final fidelity (both the quantum and the classical) decreases as L increases and increases as p increases. We can also see that it is much easier for a near-perfect reconstruction of the probability distribution than the construction of the underlying quantum state, as in the numerical simulations \mathcal{I}_c is always at least one order of magnitude smaller than \mathcal{I}_q . In Fig.(1)(c, d) we show the minimum number N of required training data for $\mathcal{I}_c \leq 1\%$ as a function of L and p respectively. We can see that N increases as L increases and decreases as p increases, as shown in Fig. 1(a, b).

Next we fix $L = 6$ and investigate the variations of \mathcal{I}_q and \mathcal{I}_c as functions of the number of sweeps, which

is shown in Fig. 2. In Fig. 2(a, c), we show \mathcal{I}_q and \mathcal{I}_c as functions of the number of sweeps when $p = 0.4$ for different values of γ , while in Fig. 2(d, f) we show \mathcal{I}_q and \mathcal{I}_c as functions of the number of sweeps when $p = 0.6$ for different values of γ . We can see that for both noise strengths, \mathcal{I}_c converges in about 1000 sweeps and \mathcal{I}_q does not fully converge after 4000 sweeps. The final values of \mathcal{I}_q and \mathcal{I}_c after 4000 sweeps are also shown in Fig. 2(e) for $p = 0.4$ and in Fig. 2(f) for $p = 0.6$. We can see that in both cases \mathcal{I}_c is about two orders of magnitude smaller than the corresponding \mathcal{I}_q and that \mathcal{I}_q and \mathcal{I}_c for $p = 0.6$ is smaller than those for $p = 0.4$.

Next we explore the learning accuracy as a function of the bond dimension D used in our ansatz. The bond dimension of the MPS corresponds to the number of singular values retained in the process of restoring the original density matrix after matrix SVD. In our case the ground state can be represented as an MPS with a certain bond dimension D_0 . For a perfect training, we need to have $D \geq D_0$ since otherwise our ansatz is not expressive enough to represent the target quantum state. If D is too large and we do not have enough training data, we might have the problem of overfitting which would also result in bad learning accuracy. The dependence of the quantum and the classical infidelities as functions of D are shown in Fig. 3, where we can see that both \mathcal{I}_q and \mathcal{I}_c decrease as D increases until saturation.

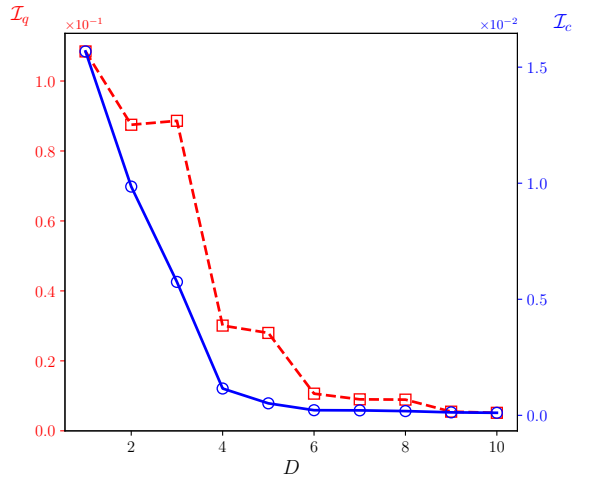


FIG. 3. \mathcal{I}_q (red dashed line with squares) and \mathcal{I}_c (blue solid line with circles) as functions of the bond dimension D . Here we have used $L = 4$, $p = 0.6$ and $N_{\text{train}} = 30000000$.

Due to the variational variational of our algorithm similar to DMRG, it could be trapped in local minima (also because the input MPS to our algorithm is randomly initialized) [35]. Therefore in our numerical results, the same reconstruction algorithm is run for many trials with random initializations of $P(\mathbf{a})$, and the one with the lowest loss value is chosen as the final result. Ideally one would likely to directly choose the trials with the high-

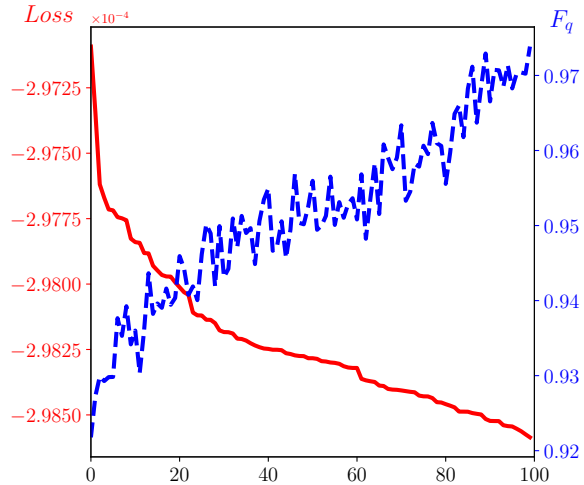


FIG. 4. The x axis denotes different labels of the 100 numerical experiments, labelled 1 to 100, sorted by their final loss values from large to small. In our simulation, we have used $P^2(\mathbf{a}) - 2P(\mathbf{a})P_s(\mathbf{a})$ as the loss value, which simply shifts the original loss value in Eq. (7) by a constant. Here the results are taken from the reconstruction of $P(\mathbf{a})$ for $L = 6$, $\gamma = 2.0$ and $p = 0.6$.

est fidelity. However in real experiment the target state is unknown and it is not possible to compute the fidelities. As a result it is important that the trials with lower loss values will correspond to those with higher fidelities. Such correspondence between loss values and fidelities is shown in Fig.(4), where we have repeated the reconstruction algorithm for 100 times. We can see that indeed the loss value has the desired correspondence with the fidelity.

Conclusion – We have presented an algorithm based on the non-negative matrix product state for quantum state tomography. Given a number of experimental measurement outcomes, our algorithm iteratively finds the optimal non-negative MPS representation which best approximates the probability distribution of these outcomes. Applying simple local transformations, the reconstructed non-negative MPS can be converted into a density matrix for the unknown quantum state, also in the MPS form. This is in comparison with the QST based on neural network states, which could easily reproduce the measurement outcomes but is often extremely difficult to directly obtain the underlying quantum state. The effectiveness of our algorithm is demonstrated with applications to the XXZ chain with depolarization noise.

CG acknowledges support from National Natural Science Foundation of China under Grants No. 11805279. DH and XW gratefully acknowledge the grant from the National Key R&D Program of China, Grant No. 2018YFA0306703.

* guochu604b@gmail.com

† xiaoting@uestc.edu.cn

- [1] A. G. White, D. F. V. James, P. H. Eberhard, and P. G. Kwiat, Nonmaximally entangled states: Production, characterization, and utilization, *Phys. Rev. Lett.* **83**, 3103 (1999).
- [2] D. F. V. James, P. G. Kwiat, W. J. Munro, and A. G. White, Measurement of qubits, *Phys. Rev. A* **64**, 052312 (2001).
- [3] F. Arute, K. Arya, R. Babbush, D. Bacon, J. C. Bardin, R. Barends, R. Biswas, S. Boixo, F. G. S. L. Brandao, D. A. Buell, *et al.*, Quantum supremacy using a programmable superconducting processor, *Nature (London)* **574**, 505 (2019).
- [4] Y. Wu, W.-S. Bao, S. Cao, F. Chen, M.-C. Chen, X. Chen, T.-H. Chung, H. Deng, Y. Du, D. Fan, *et al.*, Strong quantum computational advantage using a superconducting quantum processor, *Phys. Rev. Lett.* **127**, 180501 (2021).
- [5] Q. Zhu, S. Cao, F. Chen, M.-C. Chen, X. Chen, T.-H. Chung, H. Deng, Y. Du, D. Fan, M. Gong, *et al.*, Quantum computational advantage via 60-qubit 24-cycle random circuit sampling, *Sci. Bull.* **67**, 240 (2022).
- [6] D. Gross, Y.-K. Liu, S. T. Flammia, S. Becker, and J. Eisert, Quantum state tomography via compressed sensing, *Phys. Rev. Lett.* **105**, 150401 (2010).
- [7] W.-T. Liu, T. Zhang, J.-Y. Liu, P.-X. Chen, and J.-M. Yuan, Experimental quantum state tomography via compressed sampling, *Phys. Rev. Lett.* **108**, 170403 (2012).
- [8] A. Smith, C. A. Riofrío, B. E. Anderson, H. Sosa-Martinez, I. H. Deutsch, and P. S. Jessen, Quantum state tomography by continuous measurement and compressed sensing, *Phys. Rev. A* **87**, 030102 (2013).
- [9] C. A. Riofrío, D. Gross, S. T. Flammia, T. Monz, D. Nigg, R. Blatt, and J. Eisert, Experimental quantum compressed sensing for a seven-qubit system, *Nat. Commun.* **8**, 15305 (2017).
- [10] G. Tóth, W. Wieczorek, D. Gross, R. Krischek, C. Schwemmer, and H. Weinfurter, Permutationally invariant quantum tomography, *Phys. Rev. Lett.* **105**, 250403 (2010).
- [11] T. Moroder, P. Hyllus, G. Tóth, C. Schwemmer, A. Niggebaum, S. Gaile, O. Gühne, and H. Weinfurter, Permutationally invariant state reconstruction, *New J. Phys.* **14**, 105001 (2012).
- [12] Y. Liu, D. Wang, S. Xue, A. Huang, X. Fu, X. Qiang, P. Xu, H.-L. Huang, M. Deng, C. Guo, X. Yang, and J. Wu, Variational quantum circuits for quantum state tomography, *Phys. Rev. A* **101**, 052316 (2020).
- [13] M. Cramer, M. B. Plenio, S. T. Flammia, R. Somma, D. Gross, S. D. Bartlett, O. Landon-Cardinal, D. Poulin, and Y.-K. Liu, Efficient quantum state tomography, *Nat. Commun.* **1**, 149 (2010).
- [14] B. P. Lanyon, C. Maier, M. Holzäpfel, T. Baumgratz, C. Hempel, P. Jurcevic, I. Dhand, A. S. Buyskikh, A. J. Daley, M. Cramer, M. B. Plenio, R. Blatt, and C. F. Roos, Efficient tomography of a quantum many-body system, *Nat. Phys.* **13**, 1158 (2017).
- [15] G. Torlai, G. Mazzola, J. Carrasquilla, M. Troyer, R. Melko, and G. Carleo, Neural-network quantum state tomography, *Nat. Phys.* **14**, 447 (2018).

[16] G. Torlai and R. G. Melko, Latent space purification via neural density operators, *Phys. Rev. Lett.* **120**, 240503 (2018).

[17] J. Carrasquilla, G. Torlai, R. G. Melko, and L. Aolita, Reconstructing quantum states with generative models, *Nat. Mach. Intell.* **1**, 155 (2019).

[18] S. Ahmed, C. Sánchez Muñoz, F. Nori, and A. F. Kockum, Quantum state tomography with conditional generative adversarial networks, *Phys. Rev. Lett.* **127**, 140502 (2021).

[19] A. W. R. Smith, J. Gray, and M. S. Kim, Efficient quantum state sample tomography with basis-dependent neural networks, *PRX Quantum* **2**, 020348 (2021).

[20] T. Baumgratz, D. Gross, M. Cramer, and M. B. Plenio, Scalable Reconstruction of Density Matrices, *Phys. Rev. Lett.* **111**, 020401 (2013).

[21] J. Wang, Z.-Y. Han, S.-B. Wang, Z. Li, L.-Z. Mu, H. Fan, and L. Wang, Scalable quantum tomography with fidelity estimation, *Phys. Rev. A* **101**, 032321 (2020).

[22] A. Rocchetto, E. Grant, S. Strelchuk, G. Carleo, and S. Severini, Learning hard quantum distributions with variational autoencoders, *NPJ Quantum Inf.* **4**, 1 (2018).

[23] I. Oseledets and E. Tyrtyshnikov, Tt-cross approximation for multidimensional arrays, *Linear Algebra Appl.* **432**, 70 (2010).

[24] G. García-Pérez, M. A. Rossi, B. Sokolov, F. Tacchino, P. K. Barkoutsos, G. Mazzola, I. Tavernelli, and S. Maniscalco, Learning to measure: Adaptive informationally complete generalized measurements for quantum algorithms, *PRX Quantum* **2**, 040342 (2021).

[25] S. T. Flammia, On SIC-POVMs in prime dimensions, *J. Phys. A: Math. Gen.* **39**, 13483 (2006).

[26] H. Sosa-Martinez, N. K. Lysne, C. H. Baldwin, A. Kalev, I. H. Deutsch, and P. S. Jessen, Experimental study of optimal measurements for quantum state tomography, *Phys. Rev. Lett.* **119**, 150401 (2017).

[27] M. A. Nielsen and I. Chuang, *Quantum Computation and Quantum Information* (Cambridge University Press, Cambridge, England, 2000).

[28] J. M. Renes, R. Blume-Kohout, A. J. Scott, and C. M. Caves, Symmetric informationally complete quantum measurements, *J Math Phys* **45**, 2171 (2004).

[29] U. Schollwöck, The density-matrix renormalization group in the age of matrix product states, *Ann Phys (N Y)* **326**, 96 (2011), january 2011 Special Issue.

[30] N. Lee, A.-H. Phan, F. Cong, and A. Cichocki, Non-negative tensor train decompositions for multi-domain feature extraction and clustering, in *Neural Information Processing*, Vol. 9949, edited by A. Hirose, S. Ozawa, K. Doya, K. Ikeda, M. Lee, and D. Liu (Springer International Publishing, Cham, 2016) pp. 87–95.

[31] E. M. Shcherbakova, Nonnegative tensor train factorization with dmrg technique, *Lobachevskii J. Math.* **40**, 1863 (2019).

[32] E. Shcherbakova and E. Tyrtyshnikov, Nonnegative tensor train factorizations and some applications, in *Large-Scale Scientific Computing*, edited by I. Lirkov and S. Margenov (Springer International Publishing, Cham, 2020) pp. 156–164.

[33] D. D. Lee and H. S. Seung, Learning the parts of objects by non-negative matrix factorization, *Nature (London)* **401**, 788 (1999).

[34] S. Holtz, T. Rohwedder, and R. Schneider, The alternating linear scheme for tensor optimization in the tensor train format, *SIAM J. Sci. Comput.* **34**, A683 (2012).

[35] Z. Liu, L.-W. Yu, L.-M. Duan, and D.-L. Deng, The presence and absence of barren plateaus in tensor-network based machine learning, [arXiv:2108.08312](https://arxiv.org/abs/2108.08312) .